

ORIGINAL ARTICLE

Shoulder joint kinetics during wheelchair propulsion on a treadmill at two different speeds in spinal cord injury patients

A Gil-Agudo, A Del Ama-Espinosa, E Pérez-Rizo, S Pérez-Nombela and B Crespo-Ruiz

Department of Physical Medicine and Rehabilitation, Biomechanics and Technical Aids Unit, National Hospital for Spinal Cord Injury, SESCAM, Toledo, Spain

Study design: Prospective study using biomechanics patient data.

Objectives: To analyze shoulder joint kinetics while propelling a wheelchair placed on a treadmill and compare shoulder joint net forces and moments when changing the speed of wheelchair propulsion on the treadmill.

Setting: National Hospital for Spinal Cord Injury, Toledo, Spain.

Methods: Sixteen subjects with thoracic spinal cord injury participated. A kinematic analysis system consisting of four camcorders (Kinescan-IBV) and a kinetic device that registered the contact force of the hand on the pushrim (SMART^{Wheel}) were used. The wheelchair was propelled at 3 and 4 km h⁻¹ without any ramp. An inverse dynamic model allowed shoulder joint net forces and moments to be calculated from the contact force of the hand on the pushrim and kinematic data.

Results: Increasing propulsion speed increased most of the temporal parameters of propulsion and pushrim kinetics and shoulder joint net forces and moments. Compared with other studies that used an ergometer or dynamometer at the same speed, the magnitude of the shoulder joint net forces and moments elicited by wheelchair propulsion on the treadmill were lower than obtained by wheelchair propulsion on other devices.

Conclusion: Lower magnitude of shoulder joint forces and moments found on the treadmill may be due to the lower friction compared with the other devices reviewed. Shoulder joint forces and moments depended strongly on the propulsion speed, increasing in magnitude when speed increased from 3 to 4 km h⁻¹.

Spinal Cord (2010) 48, 290–296; doi:10.1038/sc.2009.126; published online 22 September 2009

Keywords: wheelchairs; biomechanics; shoulder; kinetics; spinal cord injuries

Introduction

The incidence of shoulder pain in people with spinal cord injury who use wheelchairs ranges from 30 to 73%.¹ Wheelchair propulsion biomechanical analysis yields pertinent information to identify the factors that predispose to such injuries.

When conducting biomechanical analysis of wheelchair propulsion, the aim is to obtain a laboratory setup that reproduces as closely as possible the conditions of wheelchair propulsion that users encounter in real life. Until now, most studies have been made by placing the wheelchair on a dynamometer² or on instrumented rollers.³ Others have designed ergometers on which the patient is placed.⁴ Considering that wheelchair propulsion on a treadmill is mechanically realistic,⁵ despite not reproducing air resistance, it is interesting that the treadmill has been used

mainly for physiological studies⁶ rather than to examine joint kinetics. The ergometer and rollers position the wheelchair so that all spatial movements except wheel rotation are disabled. An artificial setting that conditions the free movements of the wheelchair could be created. Some authors consider that wheelchair propulsion on a treadmill is the situation that most closely simulates real-life propulsion on a smooth surface.^{6,7} Given the lack of similar studies, we undertook this study to analyze shoulder kinetics while propelling a wheelchair placed on a treadmill and to compare shoulder joint net forces and moments when changing the speed of wheelchair propulsion on the treadmill. We hypothesized that

1. Shoulder joint net forces and moments found when propelling a wheelchair on a treadmill would be of lower magnitude than those found in other studies conducted on ergometers or dynamometers
2. Shoulder joint net forces and moments would vary at different speeds of propulsion

Correspondence: Dr A Gil-Agudo, Unidad de Biomecánica y Ayudas Técnicas, Hospital Nacional de Paraplégicos, Finca la Peraleda s/n, 45071 Toledo, Spain.
E-mail: amgila@sescam.jccm.es

Received 10 November 2008; revised 30 July 2009; accepted 1 August 2009; published online 22 September 2009

Table 1 Subject demographics (mean \pm s.d. if applicable)

n	16
Sex	3 Female, 13 Male
Age (years)	37.5 (9.8)
Height (m)	1.7 (0.1)
Weight (kg)	70.1 (10.9)
Injury level	T1–T12

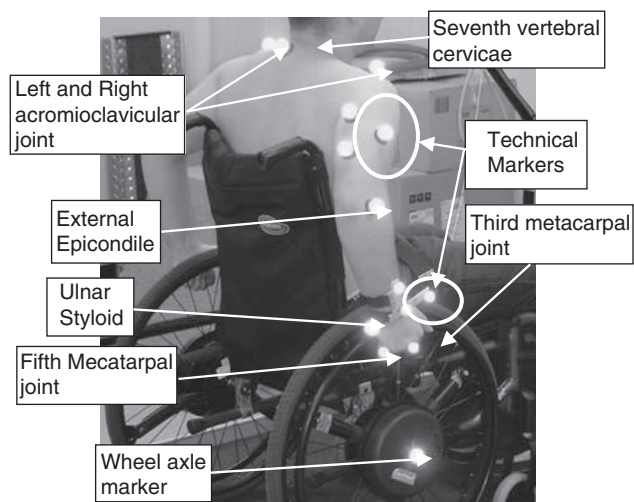


Figure 1 Marker placement: external and internal epicondyles of the elbow joint, radial and ulnar styloid process, first phalanx of fingers 2, 3 and 5. Six support markers were used, three in the upper part of the arm and three on a support placed on the distal forearm. Two support markers were positioned to identify the head of the humerus.

Materials and methods

Participants

Sixteen people who met the following criteria were enrolled:

1. Complete spinal cord injury (T1–T12), ASIA A or B
2. Duration of the injury of at least 6 months.
3. No history of shoulder pain conditions
4. No regular participation in sports activities
5. Age over 18 years and under 65 years

The demographic characteristics of these patients are shown in Table 1. All patients signed an informed consent form before the study. The guidelines of the declaration of Helsinki were followed in every case.

Kinematics

Kinematic right upper limb data were collected at a 50 Hz sampling frequency with four camcorders (Kinescan-IBV, Instituto de Biomecánica de Valencia, Valencia, Spain). Spatial marker coordinates were smoothed out using a procedure of mobile means. Reflective markers were positioned following ISB recommendations⁸ to define local reference systems on the hand, forearm and arm (Figure 1). The reference system on the trunk consisted of markers placed on the seventh cervical vertebra (C7) and on the right

(ACRR) and left (ACRL) acromioclavicular joints. The axes of this reference system were calculated as follows:

The z axis (+extension/–flexion) was formed with the right and left acromioclavicular markers:

$$\vec{z}_{\text{trunk}} = \frac{\vec{ACR}_R - \vec{ACR}_L}{\|\vec{ACR}_R - \vec{ACR}_L\|}$$

The y axis (+ rotation toward the left/–rotation toward the right) was defined as the cross product of the z axis and the vector formed by the markers on the seventh cervical vertebra and left acromioclavicular joint:

$$\vec{y}_{\text{trunk}} = \frac{(C7 - \vec{ACR}_L) \times \vec{z}_{\text{trunk}}}{\|(C7 - \vec{ACR}_L) \times \vec{z}_{\text{trunk}}\|}$$

The x axis (+ right tilt/– left tilt) was defined as the cross product of the y axis and the z axis:

$$\vec{x}_{\text{trunk}} = \frac{\vec{y}_{\text{trunk}} \times \vec{z}_{\text{trunk}}}{\|\vec{y}_{\text{trunk}} \times \vec{z}_{\text{trunk}}\|}$$

Finally, to ensure the orthogonality of the reference system of the trunk, the definitive z axis was calculated as the cross product of the x and y vectors:

$$\vec{z}_{\text{trunk}} = \frac{\vec{x}_{\text{trunk}} \times \vec{y}_{\text{trunk}}}{\|\vec{x}_{\text{trunk}} \times \vec{y}_{\text{trunk}}\|}$$

Kinetics

The wheels of the chair were replaced by two SMART^{Wheels} (Three Rivers Holdings, LLC, Mesa, AZ, USA). A synchronization pulse from the Kinescan-IBV was used to trigger the start of kinetic and kinematic collection. Kinetic data were recorded at a frequency of 240 Hz and filtered using a Butterworth, fourth-order, low-pass filter with a cutoff frequency of 20 Hz and a zero phase lag. Spatial marker coordinates were interpolated by cubic spline to synchronize with the kinetic data.

All subjects were right hand dominant. The data recorded with the right wheel were used for the kinetic analysis. The left wheel was also replaced to balance the inertia characteristics of both axes and thus ensures symmetrical propulsion.

Data compilation

A standard adjustable wheelchair, Action3 Invacare (Invacare Corp, Elyria OH, USA) was appropriately fitted for each subject and placed on a treadmill (Bonte Zwolle BV, BO Systems, Netherlands). Power output was determined in the form of a drag test in which the drag force of the wheelchair-user system was measured⁹ with a force transducer (Revere ALC 0,5. Vishay Revere Transducers BV Breda, The Netherlands). After a 2-min adaptation period, participants propelled the wheelchair at 3 km h⁻¹ during 1 min. After a resting period of 3 min, a second 1 min recording was made at 4 km h⁻¹. We used a digital slope meter (Solatronic EN 17, Fisco Tools Limited, Brook Road, Rayleigh, Essex, UK) to verify that the treadmill surface remained parallel to the

floor at all times. We conducted propulsion trials on the treadmill with a safety system. A spotter at the front of the treadmill controlled the safety tether.

Data analysis

Biomechanical model. A model of inverse dynamics was created to identify the net forces and moments exerted on the shoulder joint complex obtained from anthropometric data, pushrim kinetics and upper limb kinematics. Segment mass, segment center of mass and inertias of the hand were computed according to methods previously reported.¹⁰ In this model, body segments were considered as rigid bodies with revolution geometries of uniform constant density.

The analysis was focused on the shoulder and did not consider the movements of the scapula, clavicle and thoracic spine. The net forces and moments were transformed to the local coordinate system of the proximal segment of the shoulder joint, that is, the trunk. All shoulder joint net forces and moments were referenced to the trunk local coordinate system.^{11,12}

The forces reported constituted the reaction forces on the shoulder (upper arm over trunk), whereas the moments were reported as the action moments (trunk over upper arm). It was assumed that the force was applied at the third metacarpal as the point of hand contact.

Although a method has been described for determining the moment applied by the hand on the pushrim,¹³ in our case we chose to overlook this distinction because researchers have found that the net hand moment is negligible for simulated level propulsion.^{14,15}

Data simplification. Data were collected in the middle 20 s interval to avoid the effect of acceleration and braking. Five consecutive cycles were selected from the 20 s data recording. The cycles were normalized from 0 to 100% because the time spent in each cycle varied across individuals and across cycles. The push phase started/finished at the instant at which the propulsive moment exerted by the user during hand contact with the pushrim was higher/lower than 1 Nm. The peaks were determined for each stroke individually, and then averaged over five cycles.

Different angles related to propulsion were identified using a marker on the right wheel axis and a marker on the metacarpophalangeal joint of the third right finger (Figure 2).¹⁶ The output variables of the biomechanical model were the time-varying 3D net shoulder joint net forces and moments. We used the following sign convention for the right shoulder:

- Fx: + anterior, –posterior
- Fy: + superior, –inferior
- Fz: + lateral, –medial
- Mx: + adduction, –abduction
- My: + internal rotation, –external rotation
- Mz: + flexion, –extension.

Temporal-spatial characteristics of propulsion, pushrim forces and moments so as total force (F_{tot}) and the propulsion moment (M_p moment around the hub) were analyzed. Tangential force was obtained from the Equation

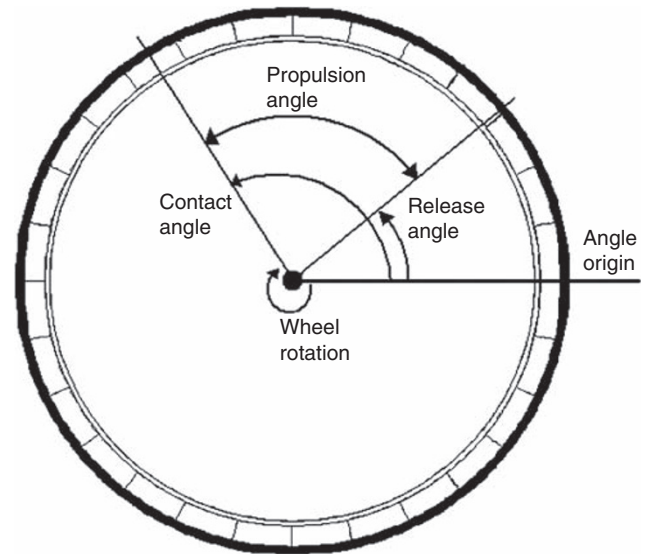


Figure 2 Description of the variables Contact Angle, Release Angle and Propulsion Angle.

$$F_t = M_p / r$$

M_p = moment around the hub
 r = pushrim radius

All the necessary equations and calculations were processed with Matlab (The Mathworks Inc., Natick, MA, USA).

Statistical analysis. Descriptive analyses were made of joint variables (mean \pm s.d.). Given the small size sample, the Wilcoxon rank test was used to detect significant differences between the mean values of the shoulder kinetic variables at the two speeds. As a non-parametric test was made, no hypothesis on the normal distribution of the variables was needed. A P -value of less than 0.05 was considered statistically significant. Analyses were made with SPSS 12.0 (SPSS Inc., Chicago, IL, USA).

We certify that all applicable institutional and government regulations concerning the ethical use of human volunteers were followed during the course of this research.

Results

The external power output yielded by the treadmill obtained with the drag test is reported in Table 2. Changing propulsion speed from 3 to 4 km h⁻¹ increased cadence, F_{tot} , F_t and M_p ($P < 0.01$), as well as the propulsion angle ($P < 0.05$), whereas the release angle decreased ($P < 0.01$) (Table 2). During the push phase, when increasing propulsion velocity, both maximal (anterior direction) and minimal peaks (posterior direction) of F_x were increased ($P < 0.01$), whereas for F_y maximal value decreased and minimal value increased its magnitude (both in inferior direction, $P < 0.05$). During the recovery phase both maximal (anterior direction) and minimal (posterior direction) F_x peaks were increased ($P < 0.01$). Maximal (lateral direction) and minimal (medial direction) peaks were also increased for F_z ($P < 0.05$; Table 3).

Table 2 Temporospacial and kinetic variables (mean \pm s.d.)

	Cadence (cycles/min)	Contact angle (degrees)	Release angle (degrees)	Propulsion angle (degrees)
3 km h ⁻¹	1.1 (0.2)**	117.5 (9.3)	51.2 (10.5)**	66.3 (16.5)*
4 km h ⁻¹	1.2 (0.3)**	115.6 (10.0)	45.8 (9.5)**	69.7 (16.8)*
	Peak total force <i>f</i> _{tot} (N)	Peak tangential force <i>F</i> _t (N)	Peak propulsion moment <i>M</i> _p (Nm)	Power output (W)
3 km h ⁻¹	58.9 (14.6)**	39.6 (9.8)**	12.6 (2.7)**	18.3 (2.7)
4 km h ⁻¹	72.8 (28.1)**	49.4 (11.6)**	15.2 (3.1)**	24.9 (3.7)

*Significantly different between the two speeds ($P < 0.05$).**Significantly different between the two speeds ($P < 0.01$).**Table 3** Peak shoulder forces acting on shoulder joint (mean \pm s.d)

	Maximum Puhs phase	P-value	Minimum Puhs phase	P-value	Maximum recovery phase	P-value	Minimum recovery phase	P-value
<i>F</i> _x (N) (+anterior, -posterior)								
3 km h ⁻¹	17.5 (10.3)	<0.01	-26.5 (10.0)	<0.01	40.8 (12.7)	<0.01	-2.1 (12.8)	<0.01
4 km h ⁻¹	37.0 (13.8)		-37.5 (11.7)		50.1 (11.6)		-7.0 (16.3)	
<i>F</i> _y (N) (+superior, -inferior)								
3 km h ⁻¹	-15.9 (8.8)	<0.05	-40.2 (7.2)	<0.05	-27.6 (5.0)	NS	-43.8 (7.7)	NS
4 km h ⁻¹	-12.0 (10.5)		-43.5 (8.5)		-25.5 (9.7)		-44.3 (8.2)	
<i>F</i> _z (N) (+lateral, -medial)								
3 km h ⁻¹	6.0 (6.2)	NS	-6.1 (5.3)	NS	7.2 (2.5)	<0.05	-6.5 (2.8)	<0.05
4 km h ⁻¹	8.0 (8.9)		-8.1 (5.1)		8.6 (4.0)		-8.5 (3.5)	

Table 4 Peak shoulder moments acting on shoulder joint (mean \pm s.d.)

	Maximum Puhs phase	P-value	Minimum Puhs phase	P-value	Maximum recovery phase	P-value	Minimum recovery phase	P-value
<i>M</i> _x (N m) (+adduction, -abduction)								
3 km h ⁻¹	0.09 (2.5)	<0.05	-4.8 (1.5)	<0.05	-2.3 (1.1)	NS	-5.0 (1.3)	<0.05
4 km h ⁻¹	1.0 (3.3)		-5.7 (1.6)		-2.0 (1.4)		-5.6 (1.6)	
<i>M</i> _y (N m) (+int. rotation, -ext. rotation)								
3 km h ⁻¹	3.1 (1.3)	<0.05	-0.3 (0.9)	NS	1.3 (0.4)	<0.05	-0.05 (0.3)	NS
4 km h ⁻¹	4.1 (1.7)		-0.3 (1.3)		1.7 (1.1)		-0.08 (0.3)	
<i>M</i> _z (N m) (+flexion, -extension)								
3 km h ⁻¹	5.7 (2.3)	<0.05	-4.1 (2.2)	NS	-0.8 (2.1)	NS	-5.9 (2.3)	NS
4 km h ⁻¹	7.9 (3.5)		-4.1 (2.5)		-1.1 (2.6)		-6.2 (2.4)	

Also, during the push phase, when increasing propulsion velocity, both maximal (adduction) and minimal (abduction) *M*_x peak values increased as well as maximal *M*_y peak (internal rotation) and *M*_z peak (flexion, $P < 0.05$). During the recovery phase, an increase was found in the minimal *M*_x peak (abduction) and in the *M*_y maximal peak (internal rotation; $P < 0.05$) as shown in Table 4.

The descriptive graphs of forces and moments evolution during the propulsion cycle can be observed in Figures 3a-c and 4a-c.

Discussion

Our two working hypotheses were confirmed. On one hand, the shoulder joint net forces and moments found were lower on the treadmill than on other devices reviewed. On the

other hand, shoulder joint net forces and moments differed between 3 and 4 km h⁻¹ speed of propulsion: most of the variables increased while increasing velocity.

A difference found with a study using a dynamometer was that the propulsion angle and maximum forces on the pushrim were lower in our sample¹⁷ but similar to the study of Veeger et al.¹⁸ In all cases, increasing the speed also increased the cadence and propulsion angle. The tangential force was lower in our study than reported previously,¹⁹⁻²¹ but the comparison is difficult because those studies related the real power output to the weight or the maximum power output, but the average conditions seems to be similar to our work. The peak shoulder posterior force in the push phase was of lower magnitude in our series than in other studies, as also occurred with the amplitude of the shoulder medial and lateral forces.^{3,11,17} The peak shoulder flexion moment during the push phase was lower than in previous studies using an ergometer.¹⁸

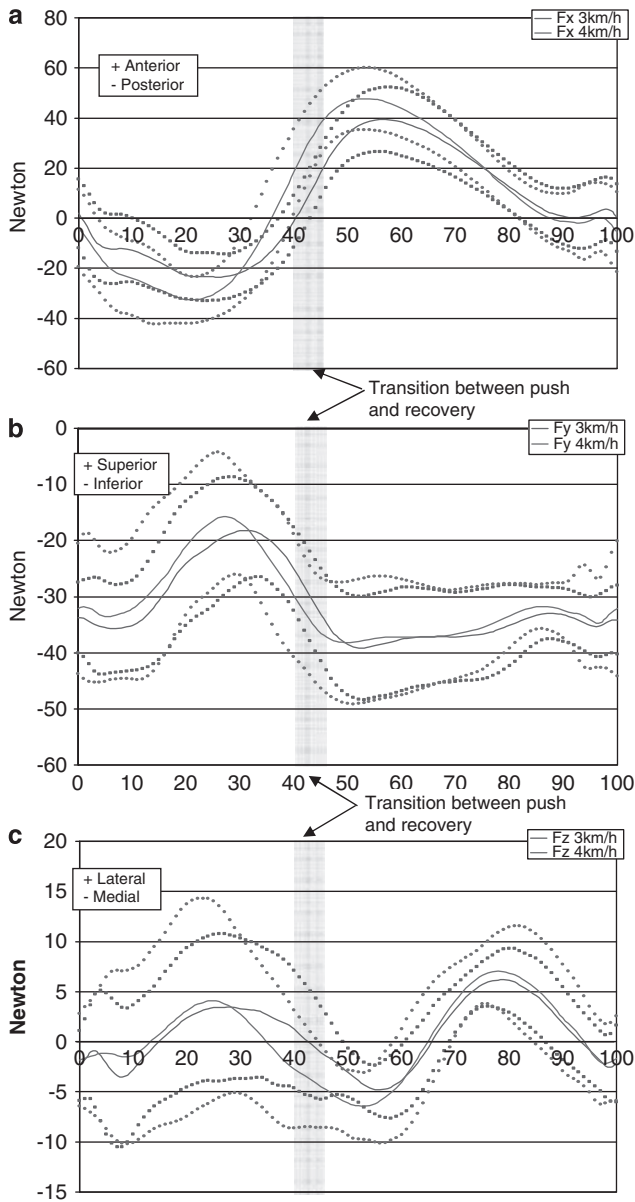


Figure 3 Illustration of the mean cycle of the shoulder joint forces in anterior–posterior (a), superior–inferior (b) and medial–lateral (c) direction throughout the cycle, in both the push phase and the recovery phase. Data obtained from all subjects. Mean (continue thick line) and s.d. (dashed line).

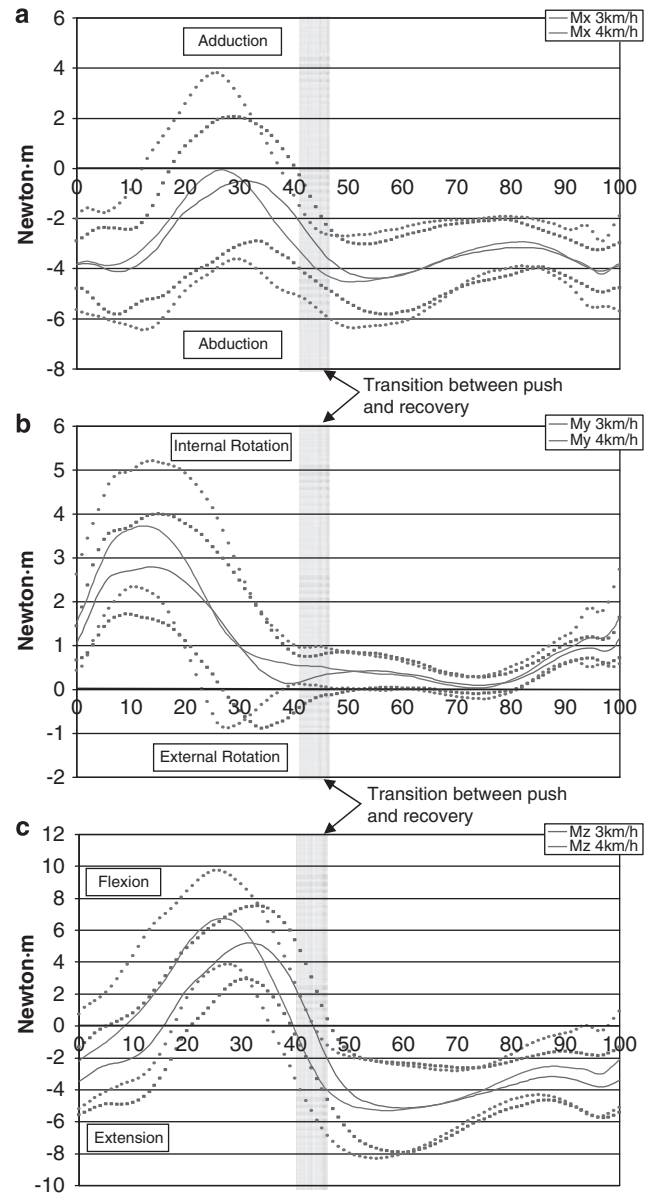


Figure 4 The mean cycle of the shoulder joint moments in the frontal (a), transversal (b) and sagittal of the trunk (c) throughout the cycle in both the push phase and the recovery phase. Data obtained from all subjects. Mean (continue thick line) and s.d. (dashed line).

We encountered difficulties in comparing the net forces and moments sustained by the shoulder joint during the act of propelling a wheelchair in different studies because of the heterogeneous methods used, to differences in laboratory equipment, use or not of subject's wheelchair, different criteria of fitting the wheelchair to the user and different calculation methods. It should be noted that the joint net moments presented in this study are referenced to the trunk coordinate system, and not to the humerus. This was done to maintain consistency in reporting shoulder joint net forces and moments in reference to the same local coordinate system. Our model does not account for the coupling

between humeral position and moment direction. Specifically, as abduction approaches 90°, a moment described as internal/external rotation in our study, may actually be more accurately described as horizontal adduction/abduction. Previous studies have reported the maximum abduction angle reached during the push phase of propulsion to be less than 40°, which lessens the effect of coupling on the results presented in this paper.^{11,12}

Analysis of the push phase disclosed that the predominant force acting on the shoulder during the push phase is posterior; when the speed increased, the vertical force was less inferior.

In previous studies, it was revealed that a positive dependence on speed for the forces at the shoulder and the predominance of a posterior force during the push phase.^{17,22} A previous study indicates that some forces acting on the shoulder in the recovery phase can be larger than those of the push phase in moderate propulsion conditions.²² It was confirmed with our results because higher anterior force peak was found during the recovery phase than posterior force peak found during the push phase. Then, it is important to study and analyze the recovery phase also, because different mechanical action can happen at the joints with some times, higher peaks than during the push phase.

We examined other studies in which data were recorded at 3 km h^{-1} , one of the speeds used in our study.^{11,17,18,21,22} Our findings coincided with most studies in that the shoulder joint net forces and moments depended strongly on the propulsion speed. In this study with a treadmill, shoulder joint net forces and moments increased when speed increased from 3 to 4 km h^{-1} , as previously reported with a dynamometer^{17,22} or ergometer.¹⁸

Groups that used a roller ergometer and groups that used a dynamometer find that the vertical component of the force in the push phase changes direction, passing from inferior to discretely superior.^{3,22} No superior forces were obtained in this study. This finding, together with the predominance of the posterior force in the push phase, indicates that pushing occurred as the result of a predominantly posterior action on the shoulder.

In the push phase, we found that the predominant moment was shoulder flexion, as in the studies consulted, but of less magnitude. With regard to the frontal plane of the trunk, we observed that the moment of abduction of the push phase decreased in magnitude but did not reach the moment of adduction, in contrast with other studies.^{3,11,17,18,22} Internal rotation predominated in our series, but the values were of lower magnitude than in other studies.^{17,18,22}

We consider that the lower magnitude of our results may be due to two factors. On the one hand, the treadmill may produce less friction than the other devices reviewed and, on the other hand, the wheelchair propulsion was more conservative to avoid striking against the side bars of the treadmill. However, it would be useful to determine the degree of friction of the treadmill to compare it with other equipment.

Conclusions

When the wheelchair was propelled on the treadmill, the magnitude of the shoulder joint net forces and moments was lower than when the wheelchair was propelled on other devices.

Shoulder joint net forces and moments depended strongly on the propulsion speed, increasing in magnitude when speed increased from 3 to 4 km h^{-1} .

Conflict of interest

These authors declare no conflict of interest.

Acknowledgements

We thank Dr Antonio Sánchez-Ramos (Head of Department of Physical Medicine and Rehabilitation) for facilitating our work. We thank José Luis Rodríguez-Martín for his critical review of the article and methodology recommendations. We also thank Elena Díaz Domínguez for her contributions to the statistical analysis, and to Barbara Thomas for the revision of this article in English. This work was part of a project financed by the Health Council of Castile-La Mancha, which does not have any commercial interest in the results of this investigation.

References

- 1 Sie IH, Waters RL, Adkins RH, Gellman H. Upper extremity pain in the postrehabilitation spinal cord injured patient. *Arch Phys Med Rehabil* 1992; **73**: 44–48.
- 2 DiGiovine CP, Cooper RA, Boninger ML. Dynamic calibration of a wheelchair dynamometer. *J Rehabil Res Dev* 2001; **38**: 41–55.
- 3 Kulig K, Rao SS, Mulroy SJ, Newsam CJ, Gronley JK, Bontrager EL *et al*. Shoulder joint kinetics during the push phase of wheelchair propulsion. *Clin Orthop* 1998; **354**: 132–143.
- 4 Niesing R, Eijskoot F, Kranse R, den Ouden AH, Storm J. Computer-controlled wheelchair ergometer. *Med & Biol Eng & Comput* 1990; **28**: 329–338.
- 5 Van Ingen Schenau GJ. Cycle power: a predictive model. *Endeavour* 1988; **12**: 44–47.
- 6 van der Woude LHV, Veeger HEJ, Dallmeijer AJ, Janssen TWJ, Rozendaal LA. Biomechanics and physiology in active manual wheelchair propulsion. *Med Eng Phys* 2001; **23**: 713–733.
- 7 Richter WM, Rodriguez R, Woods KR, Axelson PW. Stroke pattern and handrim biomechanics for level and uphill wheelchair propulsion at self-selected speeds. *Arch Phys Med Rehabil* 2007; **88**: 81–87.
- 8 Wu G, van der Helm F, Veeger HEJ, Makhssous M, Van Roy P, Anglin C *et al*. ISB recommendation on definitions of joint coordinate systems of various joints for the reporting of human joint motion- Part II: shoulder, elbow, wrist and hand. *J Biomechanics* 2005; **38**: 981–992.
- 9 Van der Woude LHV, De Groot G, Hollander AP, van Ingen Schenau GJ, Rozendaal RH. Wheelchair ergonomics and physiology testing of prototypes. *Ergonomics* 1986; **29**: 1561–1573.
- 10 Clauser CE, McConville JT, Young JW. Weight, volume and center of mass of segments of the human body. AMRL-TR-69-70. Wright-Patterson Air Force Base, Yellow Springs (OH) 1969.
- 11 Mercer JL, Boninger M, Koontz A, Ren D, Dyson-Hudson T, Cooper R. Shoulder joint kinetics and pathology in manual wheelchair users. *Clin Biomech* 2006; **21**: 781–789.
- 12 Cooper R, Boninger M, Shimada S, Lawrence B. Glenohumeral joint kinematics and kinetics for three coordinate system representation during wheelchair propulsion. *Am J Phys Med Rehabil* 1999; **78**: 435–446.
- 13 Cooper RA, Robertson RN, VanSickle DP, Bonninger ML, Shimada SD. Methods for determining three-dimensional wheelchair pushrim forces and moments—a technical note. *J Rehabil Res Dev* 1997; **34**: 435–446.
- 14 Veeger HEJ, van der Woude LHV, Rozendaal RH. Load on the upper extremity in manual wheelchair propulsion. *J Electromyogr Kinesiol* 1991; **1**: 270–280.
- 15 VanSickle DP, Cooper RA, Boninger ML, Robertson RN, Shimada SD. A unified method for calculating the center of pressure during wheelchair propulsion. *Ann Biomed Eng* 1998; **26**: 328–336.
- 16 Davis LA, Growney ES. Three-dimensional kinematics of the shoulder complex during wheelchair propulsion: a technical report. *J Rehabil Res Dev* 1998; **35**: 61–72.
- 17 Koontz AM, Cooper RA, Boninger ML, Souza AL, Fay BT. Shoulder kinematics and kinetics during two speeds of wheelchair propulsion. *J Rehabil Res Dev* 2002; **39**: 635–650.
- 18 Veeger HEJ, Rozendaal LA, van der Helm FCT. Load on the shoulder on low intensity wheelchair propulsion. *Clin Biomech* 2002; **17**: 211–218.

- 19 Dallmeijer AJ, van der Woude LHV, Veeger HEJ, Hollander AP. Effectiveness of force application in manual wheelchair propulsion in persons with spinal cord injuries. *Am J Phys Med Rehabil* 1998; **77**: 213–221.
- 20 de Groot S, Veeger HEJ, Hollander AP, van der Woude LHV. Consequence of feedback-based learning of an effective hand rim wheelchair force production on mechanical efficiency. *Clin Biomech* 2002; **17**: 219–226.
- 21 Van Drongelen S, Van der Woude LHV, Janssen TW, Angenot E, Chadwick EK, Veeger DH. Mechanical load on the upper extremity during wheelchair activities. *Arch Phys Med Rehabil* 2005; **86**: 1214–1220.
- 22 Collinger JL, Boninger ML, Koontz AM, Price R, Sisto SA, Tolerico ML *et al*. Shoulder biomechanics during the push phase of wheelchair propulsion: a multisite study of persons with paraplegia. *Arch Phys Med Rehabil* 2008; **89**: 667–676.